Journal of Physics D: Applied Physics

PAPER • **OPEN ACCESS**

Formation and control of the E_2^* center in implanted β-Ga_2O_3 by reverse-bias and zero-bias annealing

To cite this article: C Zimmermann *et al* 2020 *J. Phys. D: Appl. Phys.* **53** 464001

OPEN ACCESS
IOP Publishing
Journal of Physics D: Applied Physics
J. Phys. D: Appl. Phys. **53** (2020) 464001 (9pp)
https://doi.org/10.1088/1361-6463/aba64d

Formation and control of the E_2^* center in implanted β-Ga_2O_3 by reverse-bias and zero-bias annealing

C Zimmermann[1], E Førdestrøm Verhoeven[1], Y Kalmann Frodason[1], P M Weiser[1], J B Varley[2] and L Vines[1]

[1] Department of Physics, Centre for Materials Science and Nanotechnology, University of Oslo, Blindern Box 1048, Norway
[2] Lawrence Livermore National Laboratory, Livermore, CA 94550, United States of America

E-mail: christian.zimmermann@fys.uio.no

Received 17 April 2020, revised 1 July 2020
Accepted for publication 15 July 2020
Published 20 August 2020

Abstract

Deep-level transient spectroscopy measurements are conducted on β-Ga_2O_3 thin-films implanted with helium and hydrogen (H) to study the formation of the defect level E_2^* ($E_A = 0.71$ eV) during heat treatments under an applied reverse-bias voltage (reverse-bias annealing). The formation of E_2^* during reverse-bias annealing is a thermally-activated process exhibiting an activation energy of around 1.0 eV to 1.3 eV, and applying larger reverse-bias voltages during the heat treatment results in a larger concentration of E_2^*. In contrast, heat treatments without an applied reverse-bias voltage (zero-bias annealing) can be used to decrease the E_2^* concentration. The removal of E_2^* is more pronounced if zero-bias anneals are performed in the presence of H. A scenario for the formation of E_2^* is proposed, where the main effect of reverse-bias annealing is an effective change in the Fermi-level position within the space-charge region, and where E_2^* is related to a defect complex involving intrinsic defects that exhibits several different configurations whose relative formation energies depend on the Fermi-level position. One of these configurations gives rise to E_2^*, and is more likely to form if the Fermi-level position is further away from the conduction band edge. The defect complex related to E_2^* can become hydrogenated, and the corresponding hydrogenated complex is likely to form when the Fermi level is close to the conduction band edge. Di-vacancy defects formed by oxygen and gallium vacancies ($V_O - V_{Ga}$) fulfill several of these requirements, and are proposed as potential candidates for E_2^*.

Keywords: β-Ga_2O_3, deep-level transient spectroscopy, hydrogen, irradiation, implantation, reverse-bias annealing, intrinsic defects

(Some figures may appear in colour only in the online journal)

1. Introduction

Monoclinic gallium sesquioxide (β-Ga_2O_3) has emerged in recent years as a promising material for applications in power electronics and UV photo-detectors due to its wide band gap and exceptionally high break-down electrical field [1–6]. There has been significant progress in improving the quality of β-Ga_2O_3 bulk crystals and thin-films [4, 7–13]. However, point defects are still a limiting factor for device

performance, and influence the operation of devices for power electronics due to, for example, Fermi-level pinning [14–16] or an increase in the on-resistance [17]. Indeed, McGlone *et al* recently showed that a defect level commonly labeled as E_2^* is limiting the device performance of metal-semiconductor field-effect transistors (MESFETs) based on β-Ga_2O_3 [14].

E_2^* is associated with a defect level at around 0.75 eV below the conduction band edge (E_C) as determined by deep-level transient spectroscopy (DLTS) [14, 15, 18–20]. The defect level has been observed in as-grown β-Ga_2O_3 thin-films deposited by plasma-assisted molecular beam epitaxy [14, 15], and is suggested to be associated with intrinsic defects due to its formation in β-Ga_2O_3 bulk crystals and thin-films upon proton irradiation [18–20]. Furthermore, the concentration of E_2^* in proton-irradiated β-Ga_2O_3 bulk crystals and thin-films increases upon heat treatments in the range of 650 K, indicating the formation of E_2^* through a thermally-activated process [19]. However, no structural origin has so far been attributed to E_2^*.

The position of the Fermi level can have a pronounced influence on defect formation processes via the contribution of the electron chemical potential to defect formation energies [21–23]. Particularly, it has been shown that several defect signatures are introduced in the space-charge region of β-Ga_2O_3 Schottky barrier diodes (SBDs) when the diodes are exposed to elevated temperatures in conjunction with an applied bias voltage, causing a change in the Fermi-level position within the space-charge region [24]. Moreover, hydrogen (H) can play an important role in defect formation because H is expected to be mobile at or slightly above room temperature in β-Ga_2O_3, and has been shown to form complexes with various acceptor defects [23, 25–27].

Here, we report on the formation of the defect level E_2^* in β-Ga_2O_3 thin-films subjected to helium- (He) and H-implantation using deep level transient spectroscopy (DLTS). We observe that the introduction of E_2^* is promoted by annealing samples subjected to H- or He-implantation under an applied reverse-bias voltage. Annealing the corresponding samples without an applied reverse-bias voltage leads to a decrease in the E_2^* concentration. Thus, annealing implanted β-Ga_2O_3 thin-films with and without an applied reverse-bias voltage can be used to control the concentration of E_2^*. Notably, a more pronounced decrease in the E_2^* concentration is seen for heat treatments without an applied reverse-bias voltage in the presence of H. We propose that E_2^* is associated with a defect complex forming more preferably when the Fermi level is further away from E_C. Importantly, at Fermi-level positions closer to E_C, a different defect complex or configuration is more likely to form that does not give rise to a charge-state transition level accessible for our DLTS measurements. Moreover, for Fermi-level positions close to E_C, H is proposed to form a hydrogenated defect complex that competes with the defect giving rise to E_2^*. Finally, based on a discussion of the present results in light of first-principles defect calculations available in the literature, di-vacancy complexes formed by oxygen vacancies (V_O) and gallium vacancies (V_{Ga}) are proposed as a promising class of candidates for E_2^*.

2. Experimental

β-Ga_2O_3 thin-films (thickness $\approx$10 μm) grown by halide vapor-phase epitaxy (HVPE) [4] on conductive β-Ga_2O_3 substrates were obtained from Novel Crystal Technology, Inc. [28]. More information regarding the morphology and microstructure of the HVPE grown β-Ga_2O_3 thin-films can be found in [4, 29, 30]. Samples measuring (5 $\times$ 5) mm^2 were cut with a laser cutter, and cleaned inside an ultrasonic bath using acetone, isopropanol and de-ionized water prior to fabricating SBDs by depositing suitable metals. The metals were deposited using e-beam evaporation, with Ti/Al (thickness = 10 nm/120 nm) serving as the Ohmic area back contact, whereas circular Ni pads (thickness = 150 nm) with diameters of 480 μm or 830 μm, respectively, were used as Schottky front contacts [31]. Per sample, around 10–15 Ni pads were deposited, i.e. 10–15 SBDs were obtained per sample.

Capacitance–voltage (CV), current–voltage (IV) and DLTS measurements were performed using a setup described in detail in [32, 33]. CV and IV measurements were performed in the dark and at room temperature. Generally, all investigated SBDs exhibited a rectification of several orders of magnitude when comparing the current at reverse and forward bias as well as very low conductance values. The depth distribution of the charge-carrier concentration (n) was computed from CV measurements [34] and is denoted as n-profile. A relative static dielectric constant (ϵ_s) of 10.2 was assumed for β-Ga_2O_3 [35].

DLTS measurements were performed in the temperature range from 290 K to 450 K during heating of the sample with 2 K min^{-1}. DLTS spectra were constructed using a lock-in (GS2) filter [34, 36]. All DLTS measurements were performed at a reverse-bias voltage of –8 V or –4 V and utilized pulse voltages of 8 V or 4 V. Parameters describing the traps present in the space-charge region, such as the trap concentration (N_t), the activation energy (E_A) and the apparent capture cross section (σ_{na}) were extracted by simulating the recorded DLTS spectra with a python-based script. From results obtained on various SBDs comprising HVPE-grown β-Ga_2O_3 thin-films, the uncertainty in E_A is estimated to be around 0.10 eV, whereas the uncertainty in σ_{na} can be expected to be within +/− an order of magnitude. Notably, using DLTS measurements, it is possible to observe comparatively low defect concentrations present in the space-charge region of SBDs [34]. Thus, DLTS measurements are particularly suitable to study the introduction of defects upon ion implantation and subsequent reverse-bias and zero-bias anneals performed on SBDs.

The setup utilized for DLTS measurements was also used for heat treatments of SBDs up to 680 K. Specifically, the heat treatments were conducted inside a metal cylinder which was evacuated using a roughing pump and a turbo pump. Thus, the anneals were performed in vacuum and in the dark. Inside

the metal cylinder, the sample was placed on a ceramic sample stage with a conductive wire in its center. For electrical contact, the sample's Ohmic area back contact was placed on top of the conductive wire, whereas one of the sample's circular Schottky front contact pads was electrically connected by placing a needle on top of the contact to be annealed. A Boonton 7200 capacitance meter was used to apply a bias voltage during the heat treatments if desired. Typical annealing experiments (annealing cycle) consisted of (i) heating the sample with a specific heating ramp to the desired annealing temperature, (ii) keeping the sample at the annealing temperature for a specific time and (iii) a cool-down of the sample with a specific cooling ramp to room temperature. The duration of the anneal refers to the time the sample was kept at the annealing temperature, excluding the time it took for heating and cooling. The heating was performed using a resistive heating element thermally connected to the sample stage, whereby the sample temperature was recorded with a calibrated thermistor placed on top of the sample stage in the vicinity of the sample. For cooling, the sample stage was brought in thermal contact with liquid nitrogen (LN_2) while the resistive heater was used to obtain the desired cooling rate. Typically, heating and cooling rates of approximately 6 K min^{-1} were utilized. Heat treatments with an applied reverse-bias voltage are denoted as reverse-bias anneals, whereas heat treatments without an applied bias voltage are referred to as zero-bias anneals. For reverse-bias anneals, a reverse bias voltage was applied during the whole annealing cycle. Unless stated otherwise, reverse-bias anneals were performed using an applied reverse-bias voltage of –8 V.

All H- and He-implantations were performed at room temperature through the Ni contacts, using kinetic energies (E) of 180 keV to 220 keV for H and 500 keV for He. The projected range (R_p) for defect generation due to the ion implantation was computed utilizing Monte-Carlo simulations as implemented within the *The Stopping and Range of Ions in Matter* package [37] using default displacement energies for Ga and O of 25 eV and 28 eV, respectively. For H implantation, R_p^H is between 850 nm and 1050 nm, whereas for He implantation, R_p^{He} is around 1150 nm. Typical ion fluences for implantation (Φ) were in the range of $5 \times 10^{12}cm^{-2} - 1 \times 10^{13}cm^{-2}$ for H and $1 \times 10^{10}cm^{-2} - 1 \times 10^{11}cm^{-2}$ for He.

3. Results and discussion

Figures 1 (a) and (b) display n-profiles recorded on a HVPE-grown β-Ga_2O_3 thin-film after He implantation, and subsequent reverse-bias and zero-bias anneals at 650 K. In figure 1 (a), results are shown for a SBD immediately after He implantation, and after reverse-bias and zero-bias anneals. After He implantation, the region around R_p^{He} is partly compensated, as evidenced by a reduction in the charge-carrier concentration. The first heat treatment leads to a restoration of the charge-carrier concentration, whereas subsequent heat treatments result only in minor changes in the n-profile, in accordance with previous reports [19, 38, 39]. In figure 1 (b), n-profiles for a second SBD on the same HVPE-grown β-Ga_2O_3 thin-film are shown. Here, results are displayed after an initial zero-bias anneal, and for subsequent reverse-bias and zero-bias anneals. The n-profiles do not change significantly after the heat treatments, which indicates that the probing depth expected for DLTS measurements (W) does not change significantly during subsequent DLTS measurements.

Figures 1 (c) and (d) show DLTS spectra recorded on the same SBDs whose n-profiles are shown in panels (a) and (b), respectively. Immediately after He implantation (see figure 1 (c)), a defect signature commonly labeled as E_2 ($E_A = 0.74$ eV, $\sigma_{na} = 1 \times 10^{-16}$ cm^2) can be seen which has previously been identified as $Fe_{GaII}^{0/-}$ (charge-state transition from neutral Fe^{3+} to an Fe^{2+} acceptor state substituting on an octahedral Ga site) [18, 33]. E_2 was also present in as-received HVPE-grown β-Ga_2O_3 thin-films (not shown), and no change is observed during the subsequent heat treatments, in accordance with previous reports [19]. Additionally, in figure 1 (c), a shoulder can be seen on the low temperature side of E_2, indicating the presence of another defect level where one would expect E_2^* to occur [18, 19]. After a subsequent reverse-bias anneal at 650 K, E_2^* ($E_A = 0.71$ eV, $\sigma_{na} = 1 \times 10^{-19}$ cm^2) is introduced with a significantly higher concentration, in accordance with the observations reported in [19]. Notably, the simulations performed to extract E_A, σ_{na} and N_t do not capture the corresponding signature entirely, indicating the presence of several overlapping defect signatures. The E_2^* concentration decreases after a subsequent zero-bias anneal at 650 K. Notably, the E_2^* concentration observed using DLTS measurements is very low, i.e. we do not expect detectable changes in the microstructure of our samples related to the formation and removal of E_2^*.

Importantly, reversing the order of the heat treatment sequence by starting with a zero-bias anneal at 650 K (see figure 1 (d)) results in a reduced introduction of E_2^* upon the initial heat treatment. The effect of reverse-bias annealing is further demonstrated by the subsequent reverse-bias anneal at 650 K, where a considerable increase in the E_2^* concentration can be observed. Interestingly, the concentration of E_2^* does not increase further when the sample is subjected to an additional reverse-bias anneal at 650 K (not shown). Moreover, the concentration associated with E_2^* can be altered by additional heat treatments: subsequent zero-bias and reverse-bias anneals at 650 K cause the concentration to decrease and increase, respectively. However, the E_2^* concentration after the second reverse-bias anneal is lower than what was observed after the first reverse-bias anneal, suggesting that the formation and removal of E_2^* is not entirely reversible. Importantly, it is not possible to decrease the E_2^* concentration by zero-bias annealing to the value which had been observed prior to the first reverse-bias anneal. This strong dependence on device history should be considered in the context of understanding the formation of E_2^* across the literature [14, 15, 18–20].

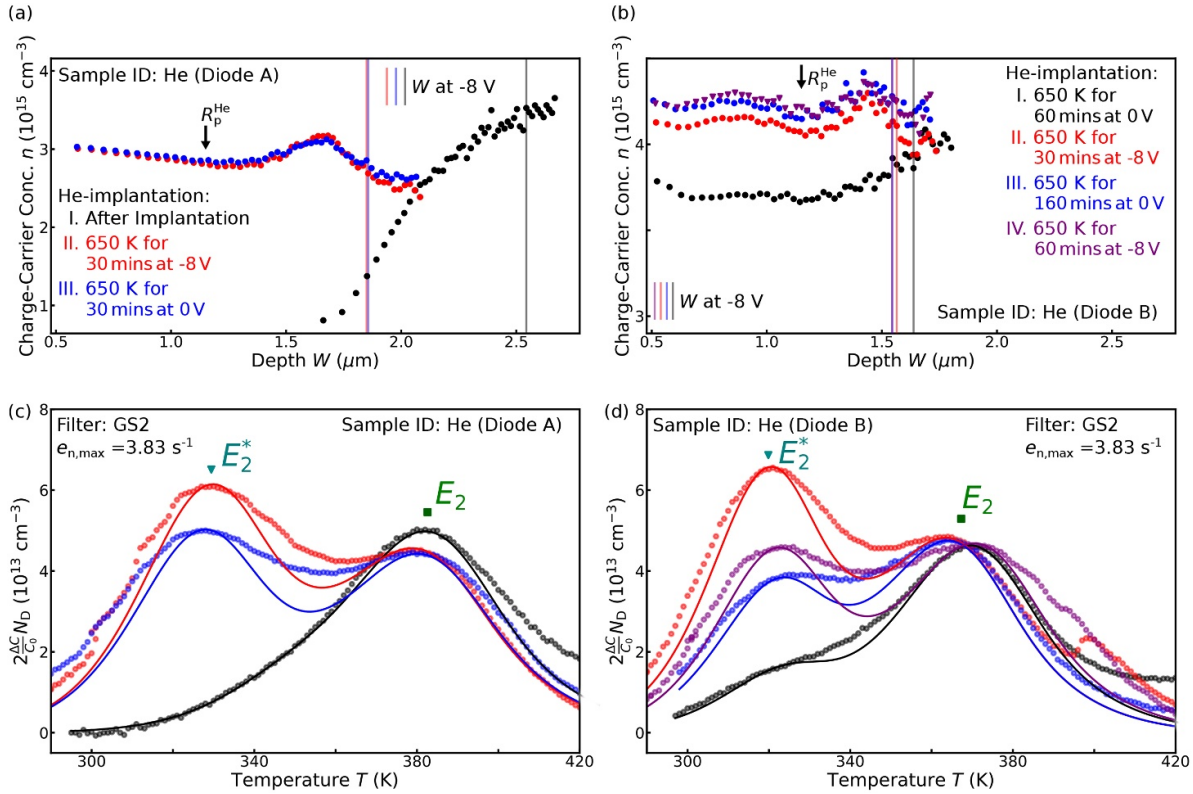

Figure 1. (a), (b) *n*-profiles and (c), (d) DLTS spectra recorded on a HVPE-grown β-Ga_2O_3 thin-film after He implantation ($E = 500$ keV, $\Phi = 2.5 \times 10^{10}$ cm^{-2}). Data (filled circles and triangles) are shown for two different SBDs located on the same HVPE-grown β-Ga_2O_3 thin-film. The SBDs were subjected to a different order of heat treatments after He implantation as listed in (a) and (b), where the order is indicated by roman letters. DLTS spectra were recorded using a reverse-bias voltage of –8 V and a pulse voltage of 8 V. R_p^{He} and the probing depth W expected in DLTS measurements are marked in (a) and (b). In (c) and (d) simulated DLTS spectra are shown as solid lines and the positions of the defect levels E_2^* and E_2 are indicated.

Next, we investigated the impact of H on the formation of E_2^*. Figure 2 shows DLTS spectra recorded on two different SBDs located on a HVPE-grown β-Ga_2O_3 thin-film subjected to H implantation and subsequent heat treatments. Figure 2 (a) shows DLTS spectra for one of the SBDs after H implantation and subsequent heat treatments at 650 K in the order: reverse-bias, zero-bias, and reverse-bias anneal. After the first reverse-bias anneal, E_2^* is seen in pronounced concentration. Subsequently, the SBD was subjected to a zero-bias anneal, and the concentration related to E_2^* is significantly lowered. Finally, the SBD was subjected to a reverse-bias anneal, and the concentration associated with E_2^* increases yet again. Interestingly, the E_2^* concentration after the second reverse-bias anneal is not as large as after the first one, and hence it seems like the introduction and removal of E_2^* is not entirely reversible regardless whether H is present or not (see figure 1). Notably, the response of E_2^* to reverse-bias and zero-bias anneals is similar for He- and H-implantation, i.e. the E_2^* concentration increases upon reverse-bias annealing, whereas it decreases due to zero-bias annealing. However, the decrease of the E_2^* concentration upon zero-bias anneals is more pronounced for the case of H implantation (see figure 2) compared to the case of He implantation (see figure 1).

In contrast to what has been observed for He implantation (see figure 1), anneals affect the E_2 concentration for H-implanted HVPE-grown β-Ga_2O_3 thin-films. Particularly, the E_2 concentration decreases due to zero-bias anneals, and increases during subsequent reverse-bias anneals. This behavior could be related to the formation and dissociation of complexes involving Fe and H [40].

Figure 2 (b) shows DLTS spectra for the H-implanted sample recorded on a second SBD subjected to a reversed order of heat treatments: zero-bias, reverse-bias, and zero-bias anneal. E_2^* is not observed when the first heat treatment is performed without an applied reverse-bias voltage. Subsequent reverse- and zero-bias anneals at 650 K cause the concentration associated with E_2^* to increase and decrease, respectively.

Further investigations were conducted by He- and subsequent H-implantation to further study the role of H, and the corresponding results are displayed in figure 3. Figure 3 (a) shows DLTS spectra recorded on a HVPE-grown β-Ga_2O_3 thin-film subjected to He- and H-implantation, and subsequent heat treatments at temperatures between 625 K and 680 K. Although E_2^* was not observed after the ion implantations or the subsequent zero-bias anneal, its concentration can be enhanced considerably by reverse-bias annealing at 625 K.

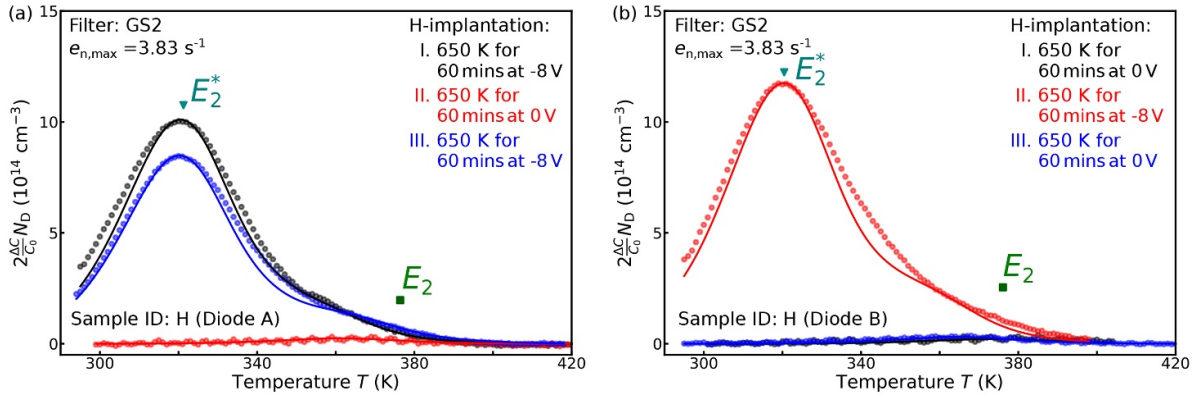

Figure 2. DLTS spectra recorded on a HVPE-grown β-Ga_2O_3 thin-film after H implantation ($E = 180$ keV, $\Phi = 1 \times 10^{13}$ cm^{-2}). Data (filled circles) are shown for two different SBDs located on the same HVPE-grown β-Ga_2O_3 thin-film. The SBDs were subjected to a different order of heat treatments after the H implantation and the order is indicated by roman letters. Simulated DLTS spectra are shown as solid lines and the positions of the defect levels E_2^* and E_2 are indicated. DLTS spectra were recorded using a reverse-bias voltage of –8 V and a pulse voltage of 8 V. The probing depth expected for the DLTS measurements did not change significantly for the different heat treatments.

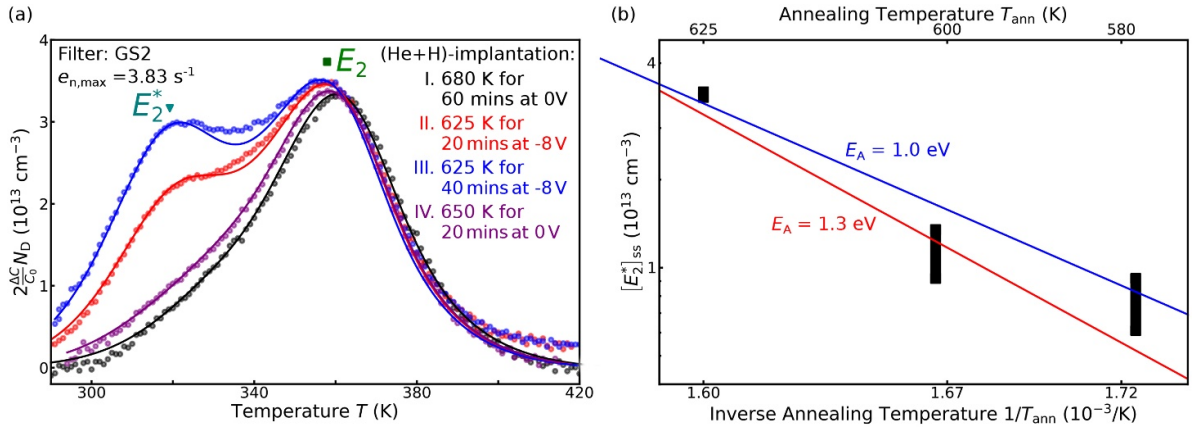

Figure 3. (a) DLTS spectra recorded on a HVPE-grown β-Ga_2O_3 thin-film after He- ($E = 500$ keV, $\Phi = 1.25 \times 10^{10}$ cm^{-2}) and H-implantation ($E = 220$ keV, $\Phi = 5 \times 10^{12}$ cm^{-2}). Data (filled circles) are shown for a SBD subjected to different heat treatments after the ion impl,antations and their order is indicated by roman letters. Notably, the annealing duration stated for step III is the accumulated annealing duration, i.e. no zero-bias anneal was performed in-between step II and III. Simulated DLTS spectra are shown as solid lines and the positions of the defect levels E_2^* and E_2 are indicated. DLTS spectra were recorded using a reverse-bias voltage of –8 V and a pulse voltage of 8 V. The probing depth expected for the DLTS measurements did not change significantly for the different heat treatments. (b) Arrhenius plot constructed using the steady-state concentrations related to E_2^* ($[E_2^*]_{ss}$) obtained by heat-treating a HVPE-grown β-Ga_2O_3 thin-film subjected to He- and H-implantation at different temperatures T_{ann} under an applied reverse-bias voltage of –8 V. From linear fits to the data (solid lines), the corresponding activation energy is estimated to be around 1.0 eV to 1.3 eV.

Subsequent reverse-bias and zero-bias anneals for the He- and H-implanted sample cause changes in the concentration of E_2^* similar to the changes observed in the H- or He-implanted samples, i.e. the concentration related to E_2^* can be increased by reverse-bias annealing and decreased by zero-bias annealing. Furthermore, the introduction of E_2^* exhibits a pronounced dependence on the duration of the reverse-bias anneal, as evidenced by the increased E_2^* concentration for the 40 min - long reverse-bias anneal as compared to the 20 min long reverse-bias anneal. When the sample receives a subsequent zero-bias anneal at 650 K, the concentration associated with E_2^* decreases. Similar to what has been observed for H implantation (see figure 2), the zero-bias anneal decreases the concentration of E_2^* to the same value that was observed prior to the initial reverse-bias anneal. Notably, no changes in the E_2 concentration are observed during zero-bias or reverse-bias anneals.

Reverse-bias anneals similar to the ones shown in figure 3 (a) were performed for annealing temperatures (T_{ann}) of 580 K, 600 K and 625 K using an applied reverse-bias voltage of –8 V. The reverse-bias anneals were conducted using different accumulated annealing durations (t_{ann}) without performing zero-bias anneals in-between the reverse-bias anneals performed at the same T_{ann}. However, zero-bias anneals were performed when switching to a different T_{ann}, i.e. the initial E_2^* concentration is nearly the same for each T_{ann}. The corresponding results were used to study the thermally-activated introduction of E_2^* assuming first order kinetics: $[E_2^*] = [E_2^*]_{ss}[1 - \exp(-kt_{ann})]$, where $[E_2^*]_{ss}$ denotes the E_2^* concentration ($[E_2^*]$) in steady-state and k denotes the

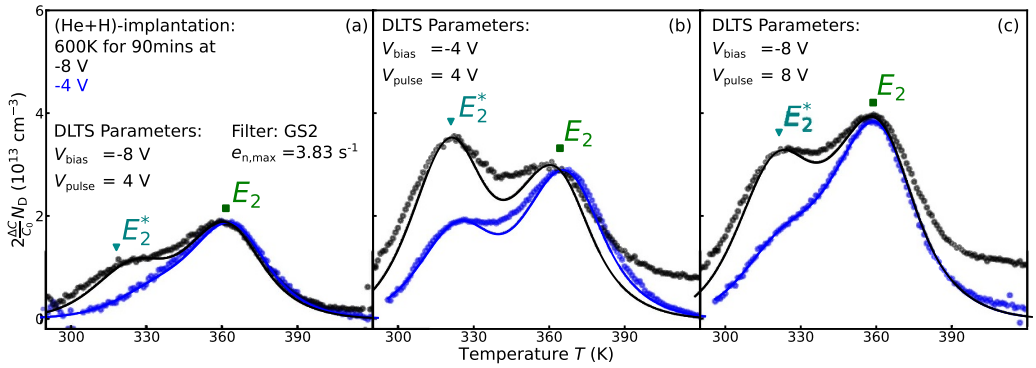

Figure 4. DLTS spectra recorded on a HVPE-grown β-Ga_2O_3 thin-film after He implantation ($E = 500$ keV, $\Phi = 1.25 \times 10^{10}$ cm^{-2}) and H implantation ($E = 220$ keV, $\Phi = 5 \times 10^{12}$ cm^{-2}) and subsequent reverse-bias anneals at 600 K for 90 min. The reverse-bias anneals were performed at –4 V (filled blue circles) and –8 V (filled black circles). Different parts of the space-charge region were probed by performing DLTS measurements using different combinations of reverse bias (V_{bias}) and pulse voltages (V_{pulse}). The respective pairs of V_{bias} and V_{pulse} are stated in the subplots. Simulated DLTS spectra are shown as solid lines and the positions of the defect levels E_2^* and E_2 are indicated.

introduction rate. Interestingly, k was found to be similar for all T_{ann} and exhibited values of around 1/3000 s^{-1}. The resulting Arrhenius plot for $[E_2^*]_{ss}$ is shown in figure 3 (b), and an activation energy of 1.0 eV to 1.3 eV was derived from linear fits to the data for the introduction of E_2^* under an applied reverse-bias voltage of –8 V. No change in the E_2^* concentration was observed for heat treatments below 500 K regardless of the kind of ion implantation or whether an external bias voltage was applied or not.

Further experiments were conducted to investigate the influence of the magnitude of the reverse-bias voltage applied during reverse-bias anneals. Figure 4 shows DLTS spectra recorded on a HVPE-grown β-Ga_2O_3 thin-film after implantation with He and H, and subsequent reverse-bias anneals at 600 K for 90 min using an applied reverse-bias voltage of either –4 V or –8 V. The reverse-bias anneal at –4 V was performed prior to the one at –8 V, and the SBD was subjected to a zero-bias anneal before performing the reverse-bias anneal at –8 V. Thus, the concentration associated with E_2^* was low prior to both reverse-bias anneals. When performing the heat treatment under a reverse-bias voltage of –8 V, the Fermi level is shifted further away from E_C inside the corresponding space-charge region, and hence in-between the surface of the HVPE-grown β-Ga_2O_3 thin-film and $W(-8\text{ V})$. Consequently, the Fermi level is affected up to a depth of $W(-4\text{ V})$ for a heat treatment under an applied reverse-bias voltage of –4 V. In figure 4 (a), DLTS measurements were performed that probe mainly the region from $W(-8\text{ V})$ to $W(-4\text{ V})$, and E_2^* is only detected in significantly increased concentration for the heat treatment performed under an applied reverse-bias voltage of –8 V. This suggests that E_2^* is only introduced inside the space-charge region established during the heat treatment. Figure 4 (b) shows DLTS spectra recorded for a probing depth between $W(-4\text{ V})$ and the surface of the HVPE-grown β-Ga_2O_3 thin-film. An increased concentration of E_2^* can be seen for the reverse-bias anneals performed at –8 V and –4 V. Importantly, the concentration related to E_2^* is significantly higher for the reverse-bias anneal performed at –8 V. In figure 4 (c), DLTS spectra are shown for a probing depth of $W(-8\text{V})$ to the surface. Although both reverse-bias anneals increase the concentration of E_2^*, the reverse-bias anneal at –8 V produces a larger concentration than the anneal at –4 V. The results presented in figure 4 show that E_2^* is introduced inside the space-charge region of SBDs subjected to reverse-bias anneals, and that applying a larger reverse-bias voltage during the heat treatments leads to the introduction of a larger amount of E_2^*, suggesting that the defect associated with E_2^* forms more preferably the further away the Fermi-level position is from E_C. The E_2 concentration is not influenced by the reverse-bias anneals. Its concentration depends, however, on the probing depth of the DLTS measurement which is most likely related to the λ-correction [34] and/or a slightly inhomogeneous depth distribution of Fe.

To summarize our findings, the formation of E_2^* after ion implantation due to a thermally-activated process suggests a relation of E_2^* to a defect complex comprising at least one intrinsic defect. This is in accordance with a previous study on proton-irradiated β-Ga_2O_3 single crystals and thin-films [19]. The formation of E_2^* is considerably enhanced by reverse-bias anneals at temperatures of around 600 K, and its formation is seen to occur inside the space-charge region of SBDs. Notably, E_2^* is introduced to a larger extent when applying larger reverse-bias voltages during reverse-bias anneals. Zero-bias anneals can be used to decrease the concentration of E_2^*. The presence of H does not significantly affect the observed introduction of E_2^*, but seems to aid the removal of E_2^* when performing zero-bias anneals.

The formation and removal behavior of E_2^* upon reverse-bias and zero-bias anneals can be explained by at least two scenarios: (i) the defect complex giving rise to E_2^* consists of constituent defects, which have a barrier for migration that depends strongly on their charge states, and hence the Fermi-level position, or (ii) the defect complex associated with E_2^* has several configurations, where only one (or a few) have a charge-state transition level giving rise to E_2^*. The configuration associated with E_2^* is more likely to form when

the Fermi level is far away from E_C, whereas configurations that do not exhibit a charge-state transition level accessible for our DLTS measurements are more favorable for Fermi-level positions close to E_C.

Scenario (i) is supported by computational studies reporting a strong dependence of the migration barrier of intrinsic defects in β-Ga_2O_3 on their respective charge state [19, 41, 42]. For example, V_O exhibits a lower migration barrier in the +2 charge state compared to the one found for the neutral charge state [42]. However, the observation of a reversible formation and removal of the defect giving rise to E_2^* is challenging to reconcile with scenario (i). Rather, one would expect that the mobile defect either leaves or enters the space-charge region during the heat treatment, and thus either the removal or formation of a defect will be observed within the space-charge region. Additionally, the dependence of the introduction of E_2^* on the magnitude of the applied reverse-bias voltage is inconsistent with scenario (i). For example, for the situation displayed in figure 4 (b), one would expect a similar E_2^* concentration to be introduced regardless of the reverse-bias voltage applied during the reverse-bias anneal. In contrast, we observed a dependence of the introduced concentration of E_2^* on the magnitude of the applied reverse-bias voltage.

Scenario (ii), however, seems to be in better agreement with the experimental observations. Within scenario (ii), it is expected that the formation and removal of E_2^* will be reversible. The degree of reversibility will, however, be influenced by other factors, e.g. the presence of other defects and the transformation dynamics between different defect configurations. The observation of a thermally-activated steady-state concentration of E_2^* also agrees with scenario (ii) where the formation and removal of E_2^* is related to a Fermi-level-dependent difference in formation energy, i.e. the equilibrium concentration of E_2^* will depend on the Fermi-level position. Thus, we also expect the formation of E_2^* to gradually depend on the magnitude of the applied reverse-bias voltage, in accordance with our observations. We derived an activation energy on the order of around 1.0 eV–1.3 eV for the thermally-activated formation of E_2^* (see figure 3 (b)). Within scenario (ii), this activation energy can be interpreted as the difference in relative formation energy between the defect configuration giving rise to E_2^* and competing defect configurations without a charge-state transition level accessible for our DLTS measurements.

The introduction of E_2^* does not seem to be influenced by the presence of H. In contrast, the removal of E_2^* due to zero-bias anneals is promoted in the presence of H. Within scenario (ii), H is proposed to form a hydrogenated version of the defect complex being connected to E_2^*, and this hydrogenated defect complex is more likely to form than the non-hydrogenated version for Fermi-level positions close to E_C. Thus, H promotes the removal of E_2^* during zero-bias annealing. For Fermi-level positions further away from E_C, the hydrogenated defect complex is not as likely to form, and thus plays only a minor or no role in the actual formation of E_2^*. Notably, for scenario (ii) to be able to explain the experimental results, the transformation between different defect configurations needs to be possible at the temperatures used for the heat treatments, whereby the kinetics of transformation may depend on the charge states of the involved defects.

Further work is necessary to identify the specific defect(s) giving rise to E_2^*. However, the formation and removal behavior of E_2^* after ion implantation and proton irradiation and the similarity in behavior seen for a wide range of different β-Ga_2O_3 samples implies the association with a defect complex either involving only intrinsic defects or comprising an intrinsic defect and an ubiquitous impurity [19]. Based on these observations, one may speculate about the origin of E_2^*. For example, di-vacancy complexes formed by V_{Ga} and V_O (V_{Ga}–V_O) possess many of the proposed features; they are intrinsic defect complexes that are expected to exhibit one or more charge-state transition levels in the proposed energy range, and they have a multitude of different configurations [19, 23]. Notably, the formation energies of various V_{Ga}–V_O complexes have been found to be comparatively low in β-Ga_2O_3, and can be expected to strongly depend on the Fermi-level position [19]. Moreover, V_{Ga}–V_O complexes display acceptor behavior for Fermi-level positions close to E_C [19], and thus hydrogenation is likely [23]. Importantly, the migration barriers computed for isolated V_{Ga} and V_O suggest that defect transformation involving vacancies will be possible at temperatures around 600 K [23, 42]. However, first-principles calculations are only reported for a few V_{Ga}–V_O configurations so far, and are not sufficient to explain the experimental observations entirely [19], which warrants further investigations.

4. Summary and conclusion

The formation and removal of E_2^* ($E_A = 0.71$ eV, $\sigma_{na} = 1 \times 10^{-19}$ cm^2) in HVPE-grown β-Ga_2O_3 thin-films subjected to ion implantation and subsequent heat treatments was studied using DLTS. The introduction of E_2^* is promoted by reverse-bias anneals at temperatures in the range of 600 K within the space-charge region of SBDs comprising the β-Ga_2O_3 thin-films subjected to He- and/or H-implantation. Subsequent zero-bias anneals at temperatures in the range of 600 K cause the concentration of E_2^* to decrease, whereby the removal of E_2^* is more pronounced if H is present in the space-charge region of the SBD. The formation of E_2^* by reverse-bias annealing is a thermally-activated process with an activation energy of 1.0 eV–1.3 eV. In summary, our results show how reverse-bias and zero-bias anneals can be used to control the concentration of E_2^* in SBDs comprising He- and/or H-implanted β-Ga_2O_3 thin-films. Importantly, it is shown that H can aid the removal of E_2^*. The results presented here strongly suggest that E_2^* is likely to form in the space-charge region of β-Ga_2O_3-based devices for power electronics if the constituent defects of E_2^* are present. Moreover, it can be expected that the E_2^* concentration will change during device operation, which suggests the importance of device preparation and measurement history in the growing number of reports about E_2^* in β-Ga_2O_3. These points are particularly relevant taking into account that E_2^* has

been shown to influence the performance of β-Ga_2O_3-based MESFETs [14, 15].

The observed formation behavior of E_2^* is explained by a change in the Fermi-level position inside the space-charge region when applying a reverse-bias voltage. Thus, we propose that E_2^* is related to a defect complex involving intrinsic defects that exhibits different configurations whose relative formation energies depend strongly on the Fermi-level position. Configurations giving rise to E_2^* are more likely to form for Fermi-level positions further away from E_C (reverse-bias annealing), whereas configurations that are preferred for Fermi-level positions close to E_C (zero-bias annealing) do not exhibit defect levels accessible for our DLTS measurements. Furthermore, E_2^* can be passivated by H, and the hydrogenated defect complex is proposed to be more likely to form for Fermi-level positions close to E_C. Divacancy complexes of the form V_{Ga}–V_O are proposed as potential candidates for E_2^*, but further experimental and computational investigations are required for an unambiguous identification of the specific structural defect associated with E_2^*.

Acknowledgment

Financial support is acknowledged from the Research Council of Norway through the FUNDAMENT project (project number: 251131), the Norwegian Micro- and Nano-Fabrication Facility (NorFab, project number: 245963) and the Faculty of Mathematics and Natural Sciences at the University of Oslo via the strategic research initiative FOXHOUND. This work was partially performed under the auspices of the U.S. DOE by Lawrence Livermore National Laboratory under contract DE-AC52-07NA27344, and supported by the Critical Materials Institute, an Energy Innovation Hub funded by the U.S. DOE, Office of Energy Efficiency and Renewable Energy, Advanced Manufacturing Office.

ORCID iDs

C Zimmermann https://orcid.org/0000-0003-3708-6074
L Vines https://orcid.org/0000-0001-5759-7192

References

[1] Higashiwaki M, Sasaki K, Murakami H, Kumagai Y, Koukitu A, Kuramata A, Masui T and Yamakoshi S 2016 Recent progress in Ga_2O_3 power devices *Semicond. Sci. Technol.* **31** 034001
[2] Nakagomi S, Momo T, Takahashi S and Kokubun Y 2013 Deep ultraviolet photodiodes based on β-Ga_2O_3/SiC heterojunction *Appl. Phys. Lett.* **103** 072105
[3] Nakagomi S, Sato T, Takahashi Y and Kokubun Y 2015 Deep ultraviolet photodiodes based on the β-Ga_2O_3/GaN heterojunction *Sensors Actuators* A **232** 208–13
[4] Mastro M A, Kuramata A, Calkins J, Kim J, Ren F and Pearton S J 2017 Perspective - Opportunities and future directions for Ga_2O_3 *ECS J. Solid State Sci. Technol.* **6** P356–9
[5] Galazka Z 2018 β-Ga_2O_3 for wide-bandgap electronics and optoelectronics *Semicond. Sci. Technol.* **33** 113001
[6] Pearton S J, Yang J, CaryIV P H, Ren F, Kim J, Tadjer M J and Mastro M A 2018 A review of Ga_2O_3 materials, processing and devices *Appl. Phys. Rev.* **5** 011301
[7] Galazka Z *et al* 2014 On the bulk β-Ga_2O_3 single crystals grown by the Czochralski method *J. Cryst. Growth* **404** 184–91
[8] Galazka Z *et al* 2017 Scaling-up of bulk β-Ga_2O_3 single crystals by the Czochralski method *ECS J. Solid. State. Sc.* **6** Q3007–Q3011
[9] Aida H, Nishiguchi K, Takeda H, Aota N, Sunakawa K and Yaguchi Y 2008 Growth of β-Ga_2O_3 single crystals by the edge-defined, film fed growth method *Japan. J. Appl. Phys.* **47** 8506–9
[10] Kuramata A, Koshi K, Watanabe S, Yamaoka Y, Masui T and Yamakoshi S 2016 High-quality β-Ga_2O_3 single crystals grown by edge-defined film-fed growth *Japan. J. Appl. Phys.* **55** 1202A2
[11] Ahmadi E, Koksaldi O S, Zheng X, Mates T, Oshima Y, Mishra U K and Speck J S 2017 Demonstration of β-$(Al_xGa_{1-x})_2O_3$/β-Ga_2O_3 modulation doped field-effect transistors with Ge as dopant grown via plasma-assisted molecular beam epitaxy *Appl. Phys. Express* **10** 071101
[12] Krishnamoorthy S, Xia Z, Bajaj S, Brenner M and Rajan S 2017 Delta-doped β-gallium oxide field-effect transistor *Appl. Phys. Express* **10** 051102
[13] Krishnamoorthy S *et al* 2017 Modulation-doped β-$(Al_{0.2}Ga_{0.8})_2O_3$/β-Ga_2O_3 field-effect transistor *Appl. Phys. Lett.* **111** 023502
[14] McGlone J F, Xia Z, Joishi C, Lodha S, Rajan S, Ringel S and Arehart A R 2019 Identification of critical buffer traps in Si δ-doped β-Ga_2O_3 MESFETs *Appl. Phys. Lett.* **115** 153501
[15] McGlone J F, Xia Z, Zhang Y, Joishi C, Lodha S, Rajan S, Ringel S A and Arehart A R 2018 Trapping effects in Si δ-doped β-Ga_2O_3 MESFETs on an Fe-doped β-Ga_2O_3 substrate *IEEE Electron Device Lett.* **39** 1042–5
[16] Huang S-S, Lopez R, Paul S, Neal A T, Mou S, Houng M-P and Li J V 2018 β-Ga_2O_3 defect study by steady-state capacitance spectroscopy *Japan. J. Appl. Phys.* **57** 091101
[17] Neal A T, Mou S, Lopez R, Li J V, Thomson D B, Chabak K D and Jessen G H 2017 Incomplete ionization of a 110 meV unintentional donor in β-Ga_2O_3 and its effect on power devices *Sci. Rep.* **7** 13218
[18] Ingebrigtsen M E, Varley J B, Yu Kuznetsov A, Svensson B G, Alfieri G, Mihaila A, Badstübner U and Vines L 2018 Iron and intrinsic deep level states in Ga_2O_3 *Appl. Phys. Lett.* **112** 042104
[19] Ingebrigtsen M E, Yu Kuznetsov A, Svensson B G, Alfieri G, Mihaila A, Badstübner U, Perron A, Vines L and Varley J B 2019 Impact of proton irradiation on conductivity and deep level defects in β-Ga_2O_3 *APL Mater.* **7** 022510
[20] Polyakov A Y *et al* 2018 Point defect induced degradation of electrical properties of Ga_2O_3 by 10 MeV proton damage *Appl. Phys. Lett.* **112** 032107
[21] Chantre A 1989 Introduction to defect bistability *Appl. Phys. Rev.* A **48** 3–9
[22] Van de Walle C G and Neugebauer Jorg 2004 First-principles calculations for defects and impurities: Applications to III-nitrides *J. Appl. Phys.* **95** 3851–79
[23] Varley J B, Peelaers H, Janotti A and Van de Walle C G 2011 Hydrogenated cation vacancies in semiconducting oxides *J. Phys.: Condens. Matter.* **23** 334212
[24] Ingebrigtsen M E, Yu Kuznetsov A, Svensson B G, Alfieri G, Mihaila A and Vines L 2019 Generation and metastability of deep level states in β-Ga_2O_3 exposed to reverse bias at elevated temperatures *J. Appl. Phys.* **125** 185706
[25] Qin Y, Stavola M, Beall Fowler W, Weiser P and Pearton S J 2019 Hydrogen centers in β-Ga_2O_3: Infrared spectroscopy

and density functional theory *ECS J. Solid. State. Sc.* **8** Q3103–Q3110
[26] Weiser P, Stavola M, Beall Fowler W, Qin Y and Pearton S 2018 Structure and vibrational properties of the dominant OH center in β-Ga_2O_3 *Appl. Phys. Lett.* **112** 232104
[27] Ritter J R, Huso J, Dickens P T, Varley J B, Lynn K G and McCluskey M D 2018 Compensation and hydrogen passivation of magnesium acceptors in β-Ga_2O_3 *Appl. Phys. Lett.* **113** 052101
[28] Novel Crystal Technology, Inc 2020 www.novelcrystal.co.jp/eng/ (Accessed: 12 February 2020)
[29] Mahadik N A, Tadjer M J, Bonanno P L, Hobart K D, Stahlbush R E, Anderson T J and Kuramata A 2019 High-resolution dislocation imaging and micro-structural analysis of HVPE-βGa_2O_3 films using monochromatic synchrotron topography *APL Mater.* **7** 022513
[30] Murakami H *et al* 2014 Homoepitaxial growth of β-Ga_2O_3 layers by halide vapor phase epitaxy *Appl. Phys. Express* **8** 015503
[31] Ingebrigtsen M E, Vines L, Alfieri G, Mihaila A, Badstübner U, Svensson B G and Kuznetsov A 2017 Bulk β-Ga_2O_3 with (010) and (201) surface orientation: Schottky contacts and point defects *Mater. Sci. Forum* **897** 755–8
[32] Svensson B G, Rydén K-H and Lewerentz B M S 1989 Overlapping electron traps in n-type silicon studied by capacitance transient spectroscopy *J. Appl. Phys.* **66** 1699–704
[33] Zimmermann C *et al* 2020 Ti- and Fe-related charge transition levels in β-Ga_2O_3 *Appl. Phys. Lett.* **116** 072101
[34] Blood P and Orton J W 1992 *The Electrical Characterization of Semiconductors: Majority Carriers and Electron States* (New York: Academic)
[35] Passlack M, Hunt N E J, Schubert E F, Zydzik G J, Hong M, Mannaerts J P, Opila R L and Fischer R J 1994 Dielectric properties of electron beam deposited Ga_2O_3 films *Appl. Phys. Lett.* **64** 2715–17
[36] Istratov A A 1997 New correlation procedure for the improvement of resolution of deep level transient spectroscopy of semiconductors *J. Appl. Phys.* **82** 2965–8
[37] Ziegler J F, Ziegler M D and Biersack J P 2010 SRIM – The stopping and range of ions in matter *Nucl. Instrum. Meth. Phys. Res.* B **268** 1818–23
[38] Wong M H, Takeyama A, Makino T, Ohshima T, Sasaki K, Kuramata A, Yamakoshi S and Higashiwaki M 2018 Radiation hardness of β-Ga_2O_3 metal-oxide-semiconductor field-effect transistors against gamma-ray irradiation *Appl. Phys. Lett.* **112** 023503
[39] Kim J, Pearton S J, Fares C, Yang J, Ren F, Kim S and Polyakov A Y 2019 Radiation damage effects in Ga_2O_3 materials and devices *J. Mater. Chem.* C **7** 10–24
[40] Higashiwaki M and Fujita S 2020 *Gallium Oxide* (Berlin: Springer)
[41] Zimmermann C, Rønning V, Frodason Y K, Varley J B, Bobal V and Vines L 2020 Primary intrinsic defects and their charge transition levels in β-Ga_2O_3 *Phys. Rev. Mater.* **4** 074605
[42] Kyrtsos A, Matsubara M and Bellotti E 2017 Migration mechanisms and diffusion barriers of vacancies in Ga_2O_3 *Phys. Rev.* B **95** 245202